

## Wireless Neural Stimulation in Freely Behaving Small Animals

Scott K. Arfin,<sup>1</sup> Michael A. Long,<sup>2</sup> Michale S. Fee,<sup>2</sup> and Rahul Sarpeshkar<sup>1</sup><sup>1</sup>Research Laboratory of Electronics, Department of Electrical Engineering and Computer Science and <sup>2</sup>Department of Brain and Cognitive Sciences, McGovern Institute for Brain Research, Massachusetts Institute of Technology, Cambridge, Massachusetts

Submitted 6 January 2009; accepted in final form 14 April 2009

**Arfin SK, Long MA, Fee MS, Sarpeshkar R.** Wireless neural stimulation in freely behaving small animals. *J Neurophysiol* 102: 598–605, 2009. First published April 22, 2009; doi:10.1152/jn.00017.2009. We introduce a novel wireless, low-power neural stimulation system for use in freely behaving animals. The system consists of an external transmitter and a miniature, implantable wireless receiver–stimulator. The implant uses a custom integrated chip to deliver biphasic current pulses to four addressable bipolar electrodes at 32 selectable current levels (10  $\mu$ A to 1 mA). To achieve maximal battery life, the chip enters a sleep mode when not needed and can be awakened remotely when required. To test our device, we implanted bipolar stimulating electrodes into the songbird motor nucleus HVC (formerly called the high vocal center) of zebra finches. Single-neuron recordings revealed that wireless stimulation of HVC led to a strong increase of spiking activity in its downstream target, the robust nucleus of the arcopallium. When we used this device to deliver biphasic pulses of current randomly during singing, singing activity was prematurely terminated in all birds tested. Thus our device is highly effective for remotely modulating a neural circuit and its corresponding behavior in an untethered, freely behaving animal.

## INTRODUCTION

The stimulation of neuronal circuits with electrical current is a highly valuable tool within the field of neuroscience. Electrical stimulation has previously been used to probe connectivity (Hahnloser et al. 2002; Swadlow 1998); to elicit (Berg and Kleinfeld 2003; Jasper and Penfield 1954) or modify (Talwar et al. 2002) certain behaviors, to bias sensory perception (Houweling and Brecht 2008; Salzman et al. 1990); or to treat a range of neurological conditions (Bittar et al. 2005; Krack et al. 2003; Moritz et al. 2008; Tarsy et al. 2008).

Standard stimulation experiments require that the subject be physically tethered to a stimulator with a bundle of electrical wires, an arrangement that has a number of practical disadvantages. For instance, the tether limits the full range of motion of the animal and can become tangled or twisted over long periods of time (Fee and Leonardo 2001). Furthermore, the tether can also cause undue stress to the animal, potentially restricting spontaneous behaviors. To avoid these issues, we designed a wireless neural stimulation system for use with freely behaving animals.

A number of major technical challenges had to be met to develop a wireless stimulator. Since the vast majority of behavioral research is conducted on small laboratory animals such as mice (30–35 g), the device has to be light enough to be easily carried. Without a wire available to provide power, an

independent power source such as a battery must be used. Unfortunately, a battery contributes a significant amount of weight, all of which must be borne by the animal. The power consumption of the implantable device must be as low as possible to minimize the size of the battery. Furthermore, removing the animal from the experiment for frequent battery changes is often not desirable.

Existing wireless stimulating devices that were assembled from commercial, off-the-shelf components were either too bulky or heavy for use with small animals or they required more power than was available from a practically sized battery (Mavoori et al. 2005; Peng et al. 2004). Other designs used application-specific integrated circuits (ASICs), which helped reduce size. However, these devices often use a transcutaneous wireless inductive power source rather than a battery (Coulombe et al. 2007; Ghovanloo and Najafi 2007; Sarpeshkar et al. 2008; Theogarajan 2008), which has a limited range (1–10 mm) that is far too small for use with freely behaving animals (Baker and Sarpeshkar 2007). In addition, the power requirements of these designs are too high for use with a battery size that is practical on small animals. Therefore we chose to explore a compact, ultra-low-power, ASIC-based implementation that could function on a tiny battery. We also designed the device to automatically enter a low-power sleep mode when not being used.

Our device was designed to limit size, weight, and power consumption. We will describe how we achieved these specifications and show the performance of the device in manipulating neural circuit dynamics and behavior in a freely moving small animal.

## METHODS

*General overview of the system design*

The wireless stimulator consists of two parts: an external transmitter, controllable through a computer interface, and a miniature, implantable wireless receiver–stimulator (Fig. 1A). A block diagram of the wireless neural stimulation system illustrates the division between external and implantable components (Fig. 1B). The implantable device is assembled on a miniature printed circuit board (PCB) and contains an off-chip receiver coil, a custom integrated circuit for data demodulation and neural stimulation, and batteries. The chip is capable of delivering biphasic current pulses to four addressable electrode sites at 32 selectable current levels ranging from 10  $\mu$ A to 1 mA. To achieve a long operating time from minimally sized batteries, an automatic standby mode decreases static power consumption during periods of inactivity. Table 1 lists the detailed specifications of the device including size, weight, power, stimulus capabilities, and lifetime.

Address for reprint requests and other correspondence: R. Sarpeshkar, Research Laboratory of Electronics, Department of Electrical Engineering and Computer Science, Massachusetts Institute of Technology, 32-294, 77 Massachusetts Ave., Cambridge, MA 02139 (E-mail: rahuls@mit.edu).

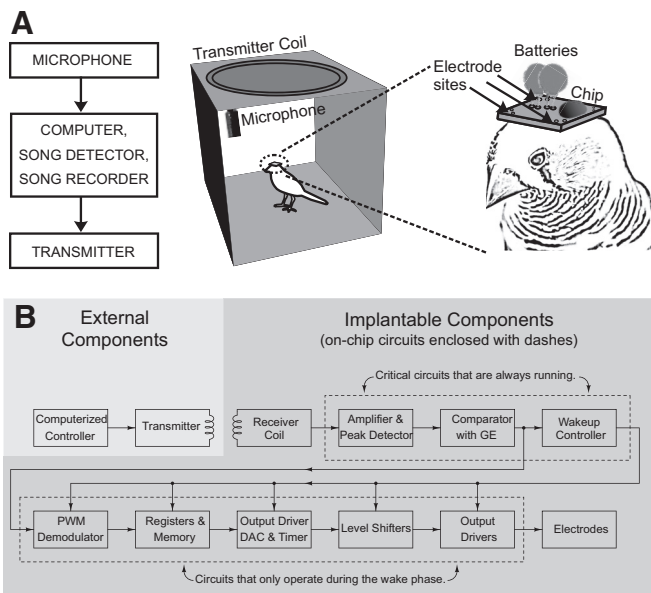


FIG. 1. The wireless stimulator. *A*: a broad overview of the wireless neural stimulation system showing the bird cage, external transmitter, and bird with implantable device. In behavioral experiments, the system was used with a microphone and a song detector to automatically operate the stimulation device during singing. Also shown is a close-up of the implanted stimulation device mounted atop the head of a zebra finch with the chip, batteries, and electrode sites (4 sites total, one per corner). *B*: a complete block diagram of the wireless neural stimulation system.

#### Data transmission using magnetic near-field radio-frequency telemetry

Data are transmitted via a near-field, magnetic link. The transmitter coil is a part of a resonant Colpitts oscillator-transmitter circuit (Fig. 2A). The transmitter is positioned externally, just outside the animal's cage (Fig. 1A).

The receiver is able to pick up only a small fraction of the total magnetic flux generated by the transmitter. A preamplifier (Fig. 2B), which provides both passive and active gain, amplifies the received signal to suitable levels. The output of the preamplifier is used to drive the input of a peak detector (not shown), which recovers the modulation input used at the transmitter. A comparator (not shown) is used to restore the peak detected waveform to a full-scale digital signal ( $V_{comp}$ ).

TABLE 1. Wireless neural stimulator specifications

| Property  | Value                                      |
|---|--|
| Board dimensions  | 1.3 × 1.3 cm                               |
| Mass with batteries   | 1.3 g                                      |
| Stimulation sites   | 4, bipolar                                 |
| Stimulation range   | 0.1–1 mA in 32 steps                       |
| Stimulation duration  | 180 $\mu$ s/phase, biphasic                |
| Maximum stimulation range                                       | 1,400 Hz                                   |
| Electrode voltage compliance                                    | 5 V  |
| Power consumption, standby                                      | 20 $\mu$ W                                 |
| Power consumption, awake  | 50 $\mu$ W                                 |
| Power-up time   | About 30 $\mu$ s                           |
| Operating time  | About 12 days (typical conditions)         |
| Transmitter range (16-V power supply, 272-mW power consumption) | 20 cm (typical)                            |
| Transmitter coil diameter                                       | 17 cm                                      |
| Bird cage interior dimensions                                   | 18 × 18.7 × 15 cm (width × depth × height) |
| Chip fabrication process  | AMI 0.5 $\mu$ m, CMOS                      |

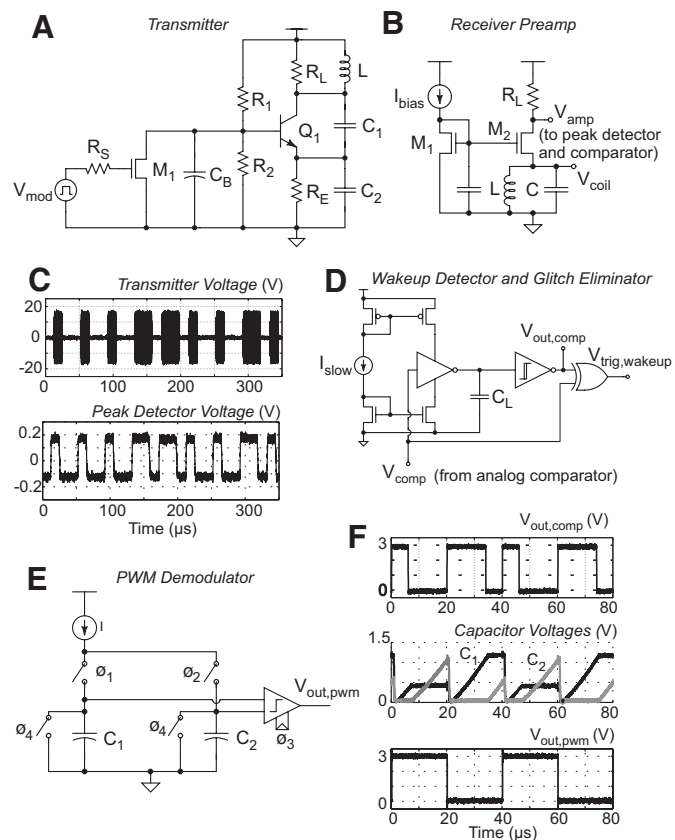


FIG. 2. Wireless data transmission and reception. Circuit schematics are given for the Colpitts oscillator-transmitter circuit (*A*), the receiver preamplifier circuit (*B*), the XOR (“exclusive or”)-based “wakeup” detector circuit with glitch eliminator (*D*), and the simplified pulse-width modulator (PWM) demodulator (*E*). *C*, top: modulated voltage at the output of the radio-frequency (RF) transmitters. Bottom: the output of the peak detector, showing the recovered amplitude-modulated (AM) signal of the carrier. *F*: example of the PWM demodulator operating.  $V_{comp}$  is a thresholded version of the peak detector voltage (*C*).  $V_{out,comp}$  is the same as  $V_{comp}$ , but with glitches removed (*D*). The PWM demodulator converts the timing of  $V_{out,comp}$  into analog voltages stored on capacitors  $C_1$  and  $C_2$ . Comparison of the 2 capacitor voltages at the end of each period determines  $V_{out,pwm}$ , which always lags  $V_{out,comp}$  by a full data period.

Data are encoded in two layers. First, a digital data sequence is pulse-width modulated (PWM), a self-clocking return-to-zero coding scheme. The PWM signal is then fed to the transmitter, which on–off keys a sinusoidal carrier. Although PWM consumes additional bandwidth through return-to-zero modulation, it is advantageous in a low-power system because complicated clock recovery circuits are unnecessary.

The choice of near-field coupling is important for saving power because low carrier frequencies (13.5 MHz) can be used. Although low carrier frequencies can restrict bandwidth, the bandwidth requirements for this neural stimulation application are low because only a limited set of stimulation commands need to be transmitted infrequently. With a data rate of 25 kbps, a stimulation triggered on 16 bits of data requires a latency of about 700  $\mu$ s.

It should be noted that near-field magnetic coupling is directional. However, there are no blind spots in the cage for reasonable orientations of the headstage. We tested the device for the maximum possible range (vertical distance from the transmitter) at three possible tilt angles (0, 45, and 60°) and two possible horizontal positions [0 cm (on-axis with the center of the transmitter coil) and 8.5 cm (the edge of the transmitter coil)]. The results indicate a maximum range of 24 cm and a range of 14.5 cm at a horizontal displacement of 8.5 cm and

a tilt angle of 60°, a considerably awkward and unlikely position for the bird. Thus even under extreme conditions, the stimulation device still has 14.5 cm of vertical range. For typical conditions, the range of the transmitter and receiver is about 20 cm.

The circuit topologies are also robust to large signals. For example, should the bird closely approach the transmitter coil, the received signal may become so large that preamplification is no longer necessary. However, the circuit topology can handle large signals easily because the output of the preamplifier stage will simply saturate at the power supply level if the input is large. The subsequent peak detected levels are thus limited as well.

### Low-power sleep mode

To conserve power when stimulation is not needed, the receiver chip automatically enters into a low-power sleep mode, where all circuits are shut down except for the preamplifier, peak detector, and comparator, which run continuously, awaiting any radio-frequency (RF) signal from the transmitter. The wakeup controller with glitch eliminator (GE) (Fig. 2D) continuously monitors the comparator output, checking for level transitions. When a transition is detected, a digital timer is reset to its highest value and all the remaining circuitry on the chip is powered up. The timer is constantly reset with every level transition of the incoming data. If no data are received for 1 s, the timer expires and the chip powers down. This circuit allows the chip to wake up remotely and immediately on the first data bit.

We have operated the implanted device on a single battery charge for  $\leq 8$  days without completely discharging the batteries. The device can be used theoretically  $\leq 15$  days on standby based on battery-capacity and power-consumption figures. For experiments with frequent stimulation (e.g., 100- $\mu$ A stimuli of five pulses each to four electrodes, 5,000 times per day, 1,000 sleep/wake cycles), power consumed by the output stage reduces running time by about 15% from the standby time alone. The additional power consumed comes from the bias current for the output driver circuits as well as the stimuli themselves. In the worst case with 1-mA pulses, running time may be reduced by about 60%.

### Data demodulation and decoding

The receiver chip is equipped with a PWM demodulation circuit (Fig. 2E). The circuit determines in a given bit period whether  $V_{out,comp}$  was logical high for greater than or less than half of the period (Fig. 2F). A bit period starts with a rising edge of  $V_{out,comp}$  and ends on a subsequent rising edge of  $V_{out,comp}$ . Thus the demodulated data ( $V_{out,pwm}$ ) contain half of the number of transitions as  $V_{out,comp}$  and every falling edge of  $V_{out,comp}$  occurs only after  $V_{out,pwm}$  has reached a stable value. For this reason, falling edges of  $V_{out,comp}$  are used to subsequently "clock"  $V_{out,pwm}$  into a shift register. The shift register converts serial data into parallel words. These words configure a DAC (D/A converter), which sets the stimulation current level, selects a specific output driver, and triggers a timer circuit, initiating a biphasic current pulse on the desired electrode pair at the chosen current level.

### Electrical stimulation

There are four output driver cells on the chip, one for each pair of electrodes. The output driver circuit implements a floating bipolar current source (McDermott 1989). The chip has one central DAC circuit that sets a reference current used to generate the actual stimulation current. A set of current mirrors copy the DAC current to the appropriate output driver transistors. Although only one output driver can be active at a time, new data can be transmitted to the chip while simultaneously delivering a stimulation charge, making it possible to stimulate multiple times in rapid succession at either the same or different sites. Off-chip series DC (low-frequency) blocking capaci-

itors are installed on the circuit board between the electrode drivers and the electrodes to prevent tissue damage (Brummer and Turner 1977).

It should be noted that data transmission is asynchronous and not continuous, meaning that data are transmitted only when stimulation is required. Further, the receiver circuit has no knowledge of when a transmission will begin. For this reason, a unique recognition sequence is used at the start of every transmission to allow the receiver to determine which bits are valid and when. A parity check also detects errors and ignores stimulation requests that contain errors. Errors are rare but become more common as the receiver moves out of range of the transmitter. In addition, spacer bits must be transmitted to prevent intended data from mimicking the recognition sequence.

Because there is no back-telemetry from the chip to the transmitter, it is not possible to tell directly whether the stimulus was applied. To address this issue, we connected a light-emitting diode (LED) to one of the unused stimulation channels, effectively reducing the number of channels from four to three. To confirm that the device was working, we used the stimulator to turn on the LED remotely, thus giving visual confirmation that the signal was correctly received. Although this method cannot easily confirm that every individual stimulation command was correctly received, this is a useful way to allow one to periodically "check" the device to make sure it is still working.

### Detailed circuit operation

*Colpitts oscillator/transmitter (circuit: Fig. 2A; operation: Fig. 2C).* To turn the oscillator on and off,  $M_1$  is operated as a switch by the PWM data, referred to here as  $V_{mod}$ . If  $V_{mod}$  is low,  $M_1$  behaves as an open circuit and can be ignored. If  $V_{mod}$  is high,  $M_1$  turns on and creates a low impedance path to ground, rapidly discharging  $C_B$ . As the base of  $Q_1$  is brought to ground, the oscillation quickly dies. When  $M_1$  is opened,  $C_B$  begins to charge through  $R_1$  and  $R_2$ . As  $Q_1$ 's base returns to its normal operating point, the oscillation restarts. The inductor  $L$  functions both as the transmitter coil and to set the resonant frequency of the oscillation, along with capacitors  $C_1$  and  $C_2$ . A list of parts and component values is provided in Table 2. Supplemental Fig. S13 provides additional information on the creation of the PWM signals and the organization of the data packet.<sup>1</sup>

The transmitter typically operates from a relatively large power supply voltage of about 16 V. This high supply voltage is necessary to maintain a wide communication range with the stimulation device. Power consumption in the transmitter is about 270 mW, which can be supplied by wall power.

*Receiver preamplifier (circuit: Fig. 2B).* The  $LC$  circuit at the source of  $M_2$  is formed by the printed coil on the PCB as well as a surface-mount capacitor. As flux is picked up by the coil, the  $LC$  circuit resonates, providing a passive voltage gain of  $Q$  at  $V_{coil}$ , where  $Q$  is the quality factor of the tuned circuit, about 25. The signal at  $V_{coil}$  is then amplified by  $M_2$  functioning as a common-gate amplifier with output  $V_{amp}$ . The amplifier is biased by the current mirror  $M_1-M_2$ , as the inductor  $L$  is a short circuit at DC. The bandwidth of the amplifier

<sup>1</sup> The online version of this article contains supplemental data.

TABLE 2. Transmitter parts list

| Part            | Value/Part Number                   |
|-----------------|-------------------------------------|
| $Q_1$           | 2N2222                              |
| $M_1$           | NDS351AN                            |
| $R_1$ and $R_2$ | 10-k $\Omega$ potentiometer         |
| $C_B$           | 1 nF                                |
| $R_L$           | Not used (replace by open circuit)  |
| $L$             | 700 nH                              |
| $C_1$           | 220 pF, tunable                     |
| $C_2$           | 680 pF                              |
| $R_S$           | Not used (replace by short circuit) |

is set by parasitic capacitance at the output of the amplifier and  $R_L$ . In this design,  $R_L$  is 80 k $\Omega$ , the bias current of  $M_2$  is 5  $\mu$ A, the overall voltage gain is 10, and the bandwidth was simulated at 30 MHz. The amplifier operates close to the MOSFET (metal-oxide-semiconductor field-effect transistor) weak inversion region, providing power-efficient voltage gain (Comer and Comer 2004; Tsividis 1999).

**Peak detector (operation: Fig. 2C) and comparator.** The peak detector circuit is similar to a source-follower, but with an intentionally small bias current and large load capacitor, forming a slow time constant. When driven with high-frequency signals beyond the linear range of the input transistor, rectification occurs. A comparator restores the peak-detected waveform to a full-scale digital signal.

**Wakeup detector and glitch eliminator (Fig. 2D).** First, any brief, spurious transitions (glitches) in the comparator output  $V_{\text{comp}}$  are removed by passing the signal through an inverter with an intentionally slow transition time. Thus brief signals are not passed by the inverter. For valid signals that do pass, the slow edges are sped up by a Schmitt trigger before entering the “exclusive or” (XOR) gate. In addition to removing glitches, the GE also introduces a delay into the comparator signal, which is necessary for the wakeup detector to work. The comparator output, along with a slightly delayed copy of itself,  $V_{\text{out,comp}}$ , is fed to an XOR gate. Whenever a transition in  $V_{\text{comp}}$  occurs,  $V_{\text{out,comp}}$  temporarily differs, causing  $V_{\text{trig,wakeup}}$  to enter the high state. This signal triggers the wakeup timer and powers up the rest of the chip if needed.

**PWM demodulator (circuit: Fig. 2E; operation: Fig. 2F).** Assume that, initially, all switches are open. The voltages on  $C_1$  and  $C_2$  are assumed to be zero. When the modulated data level ( $V_{\text{out,comp}}$ ) goes high, switch  $\phi_1$  closes and charges  $C_1$  with current  $I$ . When  $V_{\text{out,comp}}$  changes from high to low, switch  $\phi_1$  opens and  $\phi_2$  closes, charging  $C_2$  with  $I$ . At the end of the bit period, switch  $\phi_2$  opens and  $\phi_3$  momentarily goes high to latch the output of the comparator and update  $V_{\text{out,pwm}}$ . After  $V_{\text{out,pwm}}$  has been latched,  $\phi_4$  briefly closes the two reset switches to return the voltages on  $C_1$  and  $C_2$  to zero. The PWM modulator effectively converts durations into voltages and reports an output corresponding to whether the input signal ( $V_{\text{out,comp}}$ ) was predominantly high or low during a given bit period.

Additional circuitry (Fig. 1B) used includes shift registers and memory, an output driver DAC and timer, level shifters, and output drivers. The shift registers for receiving incoming data and memory for storing these data are designed from a digital standard cell library (Tanner Research, Monrovia, CA). The output driver DAC is a digitally controllable current source consisting of a set of binary weighted current sources, which are switched on or off and then combined in accordance with the stimulation parameters.

The stimulator chip requires a dual power supply. A single battery (Panasonic ML621) powers all the integrated circuits except for the output drivers, which require a larger power supply for wider voltage compliance. The dual power supply is achieved by adding an additional battery (Panasonic ML614) in series with the first battery to double the power supply. A set of level shifters amplify the output driver control signals running at the lower supply up to the level required for the higher supply.

For complete schematics of the entire custom integrated circuit, see Supplemental Figs. S1–S11.

### ASIC and PCB fabrication

The ASIC was fabricated in a 0.5- $\mu$ m CMOS (complementary metal-oxide-semiconductor) process (AMI Semiconductor, Pocatello, ID). The PCB for the stimulator chip, including receiver coil, was fabricated by Advanced Circuits (Aurora, CO). Advanced Circuits also fabricated the PCB for the transmitter circuit. Supplemental Fig. S12 provides the layout and required components for the PCB.

### Animals and surgery

Adult (>100 days post hatch) male zebra finches (*Taeniopygia guttata*) were obtained from our breeding colony or from a commercial breeder. Birds were housed under constant 12-h light/dark conditions and given unlimited food and water. All procedures described here were approved by an institutional animal care and use committee at the Massachusetts Institute of Technology.

Prior to surgery, birds were anesthetized with 1–2% isoflurane in oxygen and placed in a stereotaxic apparatus. Craniotomies were made bilaterally above HVC (1.9 to 2.7 mm lateral; 0 to 0.5 mm anterior to the bifurcation of the midsagittal sinus). Two stimulating electrode pairs (600- $\mu$ m separation), constructed from 50- $\mu$ m Teflon-coated stainless steel wire (California Fine Wire), were stripped 300  $\mu$ m at the tips and implanted to a depth of 500  $\mu$ m in each HVC. Once the electrodes were in place, the device was secured to the bird's skull with dental acrylic. After surgery, birds were placed inside sound-isolation chambers and allowed to recover and acclimate to the chamber.

### Acoustic recording and automatic electrical microstimulation

An adult male zebra finch was placed inside a sound-isolation chamber and a microphone (Audio Technica AT803B) was placed inside the chamber external to the cage. Stimulation parameters were set in advance on a computer that would generate the PWM data sequence and transfer it to the memory of an arbitrary waveform generator (Agilent 33250). The PWM data could be recalled on command and sent to the transmitter. The data transmission specifies stimulation sites, number of pulses, and pulse intensity. The neural stimulation device receives and decodes the data stream and provides the desired neural stimulation.

Sound inside the chamber was continuously monitored with Sound Analysis Pro software. When the software detected spontaneous birdsong, the sound was recorded to disk. Simultaneously, the microphone signal was sent to an external electronic circuit to also detect birdsong and trigger the wireless transmitter after a random delay. The random delay was achieved by gating the song detector output with an independent oscillator. Since singing in isolation occurs spontaneously and randomly, the bird's song will also fall into phase with the delay oscillator at random. The objective was to apply electrical stimuli to HVC approximately once per motif, at a random time within the motif<sup>2</sup>. The time of the neural stimulation was also marked onto

<sup>2</sup> The motif is a repeated unit of song substructure about 0.5–1.0 s in duration.

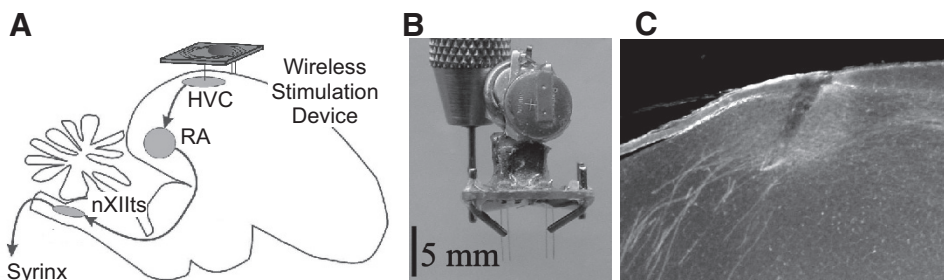


FIG. 3. Implantation of the wireless stimulator. *A*: schematic showing the stimulation device and relevant parts of the song production pathway. *B*: the device ready for implantation, showing 2 pairs of stimulating electrodes, batteries, and structural legs. *C*: dark-field microphotograph of a 100- $\mu$ m parasagittal slice of finch forebrain showing HVC, a stimulating electrode track penetrating into that nucleus, and robust nucleus of the arcopallium (RA) projecting nerve fibers (*left*).

the audio recording with an out-of-band tone so it could be identified later during analysis of the obtained recordings.

Motifs were recorded in this manner on four birds. For three of the four birds, stimuli were a train of five bipolar, biphasic (0.18 ms/phase) pulses per hemisphere at 10, 40, 70, or 100  $\mu$ A. The fourth bird was tested at only a single current level. Approximately 150 motifs were collected per bird, per level of stimulation. Motifs were analyzed using in-house computer software that computed spectral and envelope information from the sound recordings. A consistent threshold for each bird was used to segment the audio into syllables and determine their duration. Syllables were classified by hand.

Typical electrode voltages during stimulation were measured by probing the electrode attachment points on the stimulator device and captured on a Tektronix TDS3014 digital oscilloscope. In anesthetized birds, stimuli were also applied unilaterally to HVC at 1-s intervals and responses were recorded from single neurons in RA with an extracellular electrode.

### Histology

Birds were deeply anesthetized with urethane and perfused with phosphate-buffered saline and paraformaldehyde. Sections (100  $\mu$ m) were cut parasagittally with a vibrating microtome (Vibratome 1000) for verification of forebrain electrode placement. The tissue slices were imaged using dark-field microscopy (Zeiss Axioplan 2).

### Electrophysiology

Single-unit electrophysiology in RA was carried out in a manner similar to that described previously (Hahnloser et al. 2006), except these recordings were performed in anesthetized (1.0–1.5% isoflurane) zebra finches. Briefly, glass microelectrodes were fabricated on a vertical puller (Narishige PE-21) and filled with 2 M sodium acetate. Electrode tips were broken to achieve a final resistance of 10–15 M $\Omega$ . Signals were amplified using an Axoclamp 2B (Axon Instruments).

## RESULTS

### *In vivo implementation of wireless stimulator*

To test the viability of our stimulator, we used the zebra finch as our model system. The zebra finch generates a well-documented behavior (singing) that is mediated by a set of dedicated song control nuclei (Fig. 3A). Included in this motor pathway is nucleus HVC (formerly known as the high vocal center), which is a forebrain region that is critically involved in song production and timing (Fee et al. 2004; Hahnloser et al. 2002; Long and Fee 2008; Nottebohm et al. 1976), which projects to the robust nucleus of the arcopallium (RA). Previous studies have demonstrated that electrical stimuli applied to HVC have resulted in premature truncation of singing behavior (Ashmore et al. 2005; Vu et al. 1994; Wang et al. 2008). We attempted to re-create this behavioral response to test the viability of our wireless device. The device was prepared with pairs of bipolar stimulating electrodes (Fig. 3B) and implanted bilaterally into HVC (Fig. 3A). In all four birds used in behavioral experiments, electrodes were histologically confirmed to be within HVC (Fig. 3C).

### *Current source characterization and programmability*

Electrode voltage was measured in anesthetized zebra finches at the completion of the chronic trials to characterize electrode impedance (Fig. 4A). Biphasic constant-current pulses were applied to HVC and the differential electrode

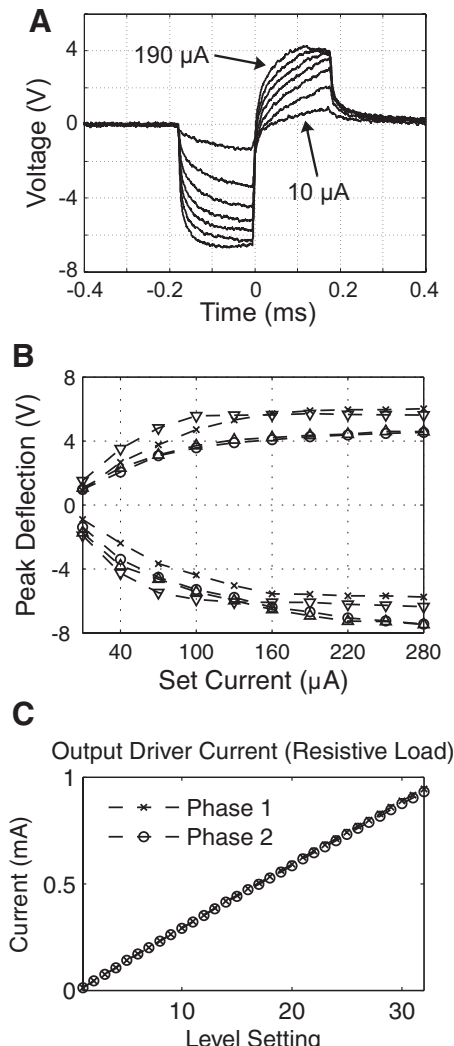


FIG. 4. Dynamic range of stimulation. A: single examples of measured electrode voltages due to unilateral stimulation of HVC. Stimulation currents ranged from 10 to 190  $\mu$ A in 30- $\mu$ A steps, with larger voltage deflections corresponding to increasing current, as shown. As stimulation current increases, the maximum electrode voltage also increases until the voltage becomes saturated at the power supply voltage. Increasing stimulation current further than shown has no significant effect on the measured electrode voltage. B: the maximum measured electrode voltage during a stimulation, as a function of current. Measurements were made for both the positive and negative phases of the same stimulation, with corresponding peaks shown with like symbols. C: the behavior of the stimulator when driving a dummy low-impedance resistive load. The current control is linear, ranging from about 10 to 940  $\mu$ A in 30- $\mu$ A steps. The positive and negative phases (Phase 1 and Phase 2) are symmetric.

voltage was recorded. As current was increased, electrode voltage also rose, indicating that raising the current level increases the intensity of the stimulation. However, current settings  $>190$   $\mu$ A caused the electrode back voltage to build quickly and reach the power supply voltage within the duration of the stimulation. As the measured voltage approaches the power supply, the current source transistors are no longer able to supply the desired current, causing the current to decrease. This loss of current control is unavoidable; however, series DC blocking capacitors in the current path guarantee that stimulations were always charge-balanced on average. Increasing the power supply voltage or decreasing electrode impedance could restore function at higher current levels.

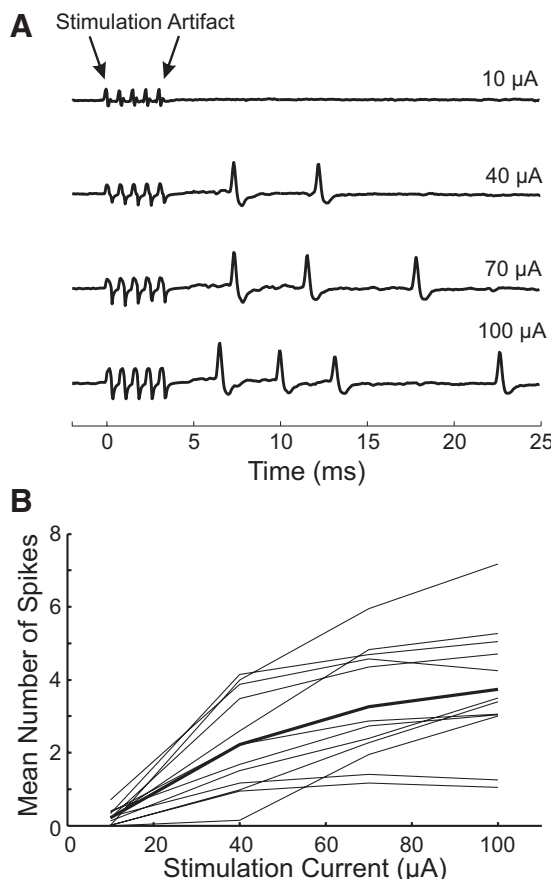


FIG. 5. Wireless stimulation strongly influences single neuron activity. *A*: example extracellular responses of an isolated RA neuron to stimulation in HVC at 4 different current levels. The stimulation artifacts have been artificially reduced in software to increase the resolution of the vertical scale. *B*: average number of spikes per response as a function of the stimulation current. Averages for 12 neurons are shown. The thick line represents the average of all neurons.

The peak voltage deflection as a function of current using four separate electrode pairs (Fig. 4*B*) shows the range of achievable currents in the implanted device. If the current level is set beyond  $130\text{ }\mu\text{A}$ , the current becomes unsustainable for the duration of the simulation because of the power supply constraint. Thus the electrode impedance can limit the range of current control in the stimulation device. To characterize the mapping from the current level setting to achieved current for ideal low-impedance electrodes, a small resistor was used as the load on the stimulation device. In this case, the current is controllable in linear steps and the positive and negative simulation phases are closely matched (Fig. 4*C*).

#### Wireless stimulation drives spiking activity in identified single neurons

We demonstrated the operation of the wireless neural stimulation system on single-neuron spiking responses in the zebra finch motor pathway. Electrical stimulation applied unilaterally to HVC resulted in time-locked spiking activity in downstream RA neurons in all cases ( $n = 4$  birds). Recordings were made from 12 RA cells at stimulation current levels of 10, 40, 70, and  $100\text{ }\mu\text{A}$  (Fig. 5, *A* and *B*). Increasing current levels caused an increase in spiking activity in all neurons tested. These

current levels are identical to those used in our behavioral experiments (see following text).

#### Wireless stimulation drives behavioral changes in the freely behaving zebra finch

Adult male zebra finch song is composed of motifs about 0.5–1.0 s in duration, which may be repeated a variable number of times (Konishi 1985). These motifs are composed of syll-

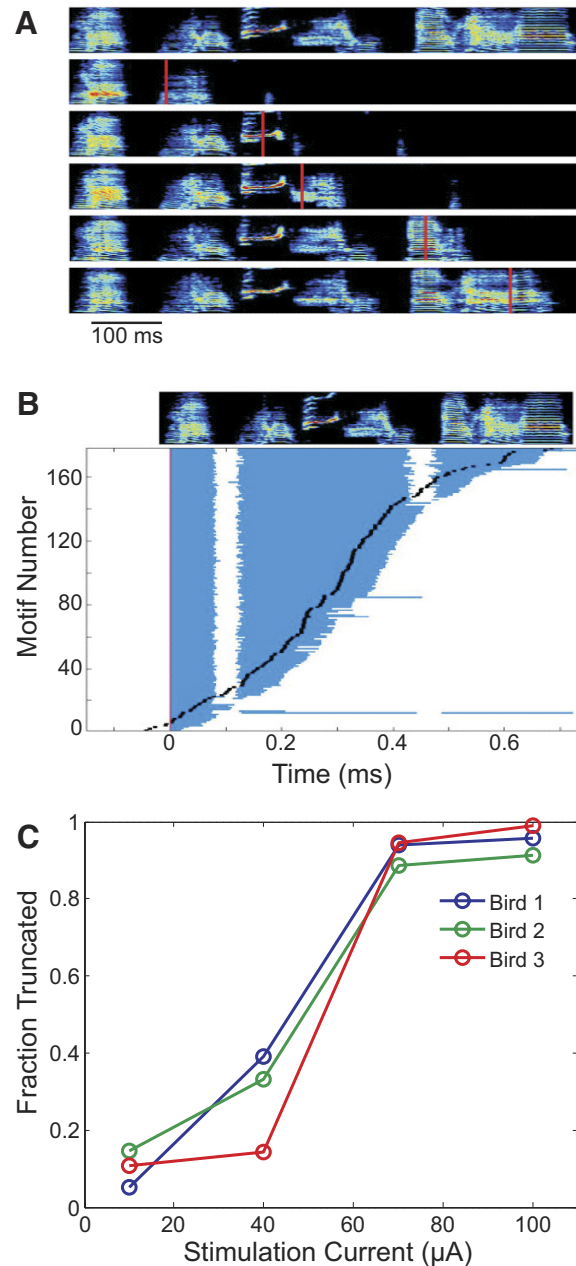


FIG. 6. Wireless stimulation strongly influences singing behavior. *A*: a sonogram of an unperturbed, reference motif is shown (*top*) followed by sonograms of 5 motifs truncated by stimulation at various points within the motif. The vertical red lines signify the time of stimulation. *B*: a raster plot showing all stimulation trials for a single bird at a current level of  $100\text{ }\mu\text{A}$ . Sound is represented by horizontal blue bars. The time of stimulation is marked (black dash) and song truncation follows after a brief delay in nearly every case. *C*: the fraction of motifs that were truncated by stimulation is shown as a function of stimulation current level ( $n = 3$  birds).

bles (periods of continuous acoustic output) about 100 ms in length. Both the individual syllable structure and the sequence of syllables comprising a motif are highly stereotyped, meaning that the zebra finch sings each motif nearly identically (Cooper and Goller 2006; Glaze and Troyer 2006). Singing may occur in the presence of a female zebra finch or spontaneously in isolation without any external stimulus (Sossinka and Böhner 1980). We exclusively studied the latter type, known as *undirected singing*.

Three adult male zebra finches (12–15 g) were implanted with the stimulation device bilaterally in HVC and subject to random electrical microstimulation triggered by singing (five biphasic pulses per hemisphere, 180  $\mu$ s per phase). Sufficiently large stimuli applied bilaterally to HVC during singing caused truncation of the ongoing motif (Fig. 6A) (Ashmore et al. 2005; Vu et al. 1994; Wang et al. 2008). On some trials, the song would start again after a brief pause (not shown).

Wireless stimulation led to current-dependent motif truncation in all birds tested (Fig. 6C). The fraction of motifs that were truncated compared with unperturbed motifs increased with increasing simulation intensity, approaching nearly 100% of motifs being truncated for stimulation intensities of  $\geq 70 \mu$ A (Fig. 6B). At this intensity, the mean time to truncation across all birds (1–3) ranged from 49.5 to 60.9 ms. A fourth bird was also implanted bilaterally in HVC, but tested at only a single stimulation intensity by setting the device at the maximum current level (1 mA), which resulted in 96% of motifs being truncated by the stimulation. The stimulation current was not measured and was most likely limited to values  $\ll 1$  mA due to power supply saturation (Fig. 4, A and B).

## DISCUSSION

The design of a low-power, miniature, implantable wireless neural stimulator for chronic use in small, freely behaving animals has been presented and tested in zebra finches. Stimulation using this wireless device led to larger electrode voltage deflections with increasing current level, increases in spiking activity within the motor pathway, and a greater incidence of motif truncation.

The small size and weight of the device are essential to its success. Small batteries, enabled by a power-conserving wakeup system, helped limit the weight. The device with batteries weighs only 1.3 g, suitable for use in rats and mice as well as songbirds. We expect that this device will be useful in wireless stimulation experiments applicable to a large body of research animals.

The introduction of this wireless stimulation device to the field of neuroscience opens up vast possibilities for behavioral experiments. For example, experiments where multiple freely behaving animals interact naturally are feasible only with a wireless system because any tethers would become entangled. Experiments that involve an animal passing freely through small openings, such as a boundary between a light and dark area, or between sections of a maze, would be limited by tethers.

The device could also be modified to suit a range of applications. For example, by adjusting the stimulus protocol, revising the circuitry to support higher current levels, and replacing the stimulating electrodes with light-emitting diodes connected to optical fibers, the device can provide optical

stimulation of neurons (Boyden et al. 2005). The higher power levels currently required for optical stimulation may result in reduced battery life. In this case, experiments using optical stimulation could be performed on a shorter timescale or the device could be used with larger batteries on animals larger than birds. Another possibility is to incorporate a scheme for wireless recharging of the batteries to extend their lifetime.

The device is also small enough that it could be chronically implanted in humans to perform deep brain stimulation (DBS). Deep brain stimulation has been shown to be effective in treating movement disorders such as Parkinson's disease and nonmovement disorders such as depression (Kringelbach et al. 2007). However, the mechanisms of DBS are not well understood. Pairing the device with simultaneous wireless micropower neural recording (Wattanapanitch et al. 2007) would make the tool even more valuable in experimental and clinical neuroscience. Further reductions in size through the use of high-precision blocking-capacitor-free stimulation (Sit and Sarpeshkar 2007) could enable scaling to applications that need large numbers of electrodes or that need to be even smaller.

## ACKNOWLEDGMENTS

We thank D. Aronov for help with some aspects of data acquisition and analysis and the anonymous reviewers for helpful comments and suggestions.

## GRANTS

This work was supported by National Institutes of Health Grants NS-056140 to R. Sarpeshkar, MH-067105 to M. S. Fee, and DC-009280 to M. A. Long and by the McGovern Institute Neurotechnology program at Massachusetts Institute of Technology.

## REFERENCES

**Ashmore RC, Wild JM, Schmidt MF.** Brainstem and forebrain contributions to the generation of learned motor behaviors for song. *J Neurosci* 25: 8543–8554, 2005.

**Baker MW, Sarpeshkar R.** Feedback analysis and design of RF power links for low-power bionic systems. *IEEE Trans Biomed Circuits Syst* 1: 28–38, 2007.

**Berg RW, Kleinfeld D.** Rhythmic whisking by rat: retraction as well as protraction of the vibrissae is under active muscular control. *J Neurophysiol* 89: 104–117, 2003.

**Bittar RG, Burn SC, Bain PG, Owen SL, Joint C, Shlugman D, Aziz TZ.** Deep brain stimulation for movement disorders and pain. *J Clin Neurosci* 12: 457–463, 2005.

**Boyden ES, Zhang F, Bamberg E, Nagel G, Deisseroth K.** Millisecond-timescale, genetically targeted optical control of neural activity. *Nat Neurosci* 8: 1263–1268, 2005.

**Brummer SB, Turner MJ.** Electrochemical considerations for safe electrical stimulation of the nervous system with platinum electrodes. *IEEE Trans Biomed Eng* 24: 59–63, 1977.

**Comer DJ, Comer DT.** Using the weak inversion region to optimize input stage design of CMOS op amps. *IEEE Trans Circuits Syst II Express Briefs* 51: 8–14, 2004.

**Cooper BG, Goller F.** Physiological insights into the social-context-dependent changes in the rhythm of the song motor program. *J Neurophysiol* 95: 3798–3809, 2006.

**Coulombe J, Sawan M, Gervais J-F.** A highly flexible system for microstimulation of the visual cortex: design and implementation. *IEEE Trans Biomed Circuits Syst* 1: 258–269, 2007.

**Fee MS, Kozhevnikov AA, Hahnloser RH.** Neural mechanisms of vocal sequence generation in the songbird. *Ann NY Acad Sci* 1016: 153–170, 2004.

**Fee MS, Leonardo A.** Miniature motorized microdrive and commutator system for chronic neural recording in small animals. *J Neurosci Methods* 112: 83–94, 2001.

**Ghovanloo M, Najafi K.** A wireless implantable multichannel microstimulating system-on-a-chip with modular architecture. *IEEE Trans Neural Syst Rehabil Eng* 15: 449–457, 2007.

**Glaze CM, Troyer TW.** Temporal structure in zebra finch song: implications for motor coding. *J Neurosci* 26: 991–1005, 2006.

**Hahnloser RH, Kozhevnikov AA, Fee MS.** An ultra-sparse code underlies the generation of neural sequences in a songbird. *Nature* 419: 65–70, 2002.

**Hahnloser RH, Kozhevnikov AA, Fee MS.** Sleep-related neural activity in a premotor and a basal-ganglia pathway of the songbird. *J Neurophysiol* 96: 794–812, 2006.

**Houweling AR, Brecht M.** Behavioural report of single neuron stimulation in somatosensory cortex. *Nature* 451: 65–68, 2008.

**Jasper H, Penfield W.** *Epilepsy and the Functional Anatomy of the Human Brain*. New York: Little, Brown and Co., 1954.

**Konishi M.** Birdsong: from behavior to neuron. *Ann Rev Neurosci* 8: 125–170, 1985.

**Krack P, Batir A, Van Blercom N, Chabardes S, Fraix V, Ardouin C, Koudsie A, Limousin PD, Benazzouz A, LeBas JF, Benabid AL, Pollak P.** Five-year follow-up of bilateral stimulation of the subthalamic nucleus in advanced Parkinson's disease. *N Engl J Med* 349: 1925–1934, 2003.

**Kringelbach ML, Jenkinson N, Owen SL, Aziz TZ.** Translational principles of deep brain stimulation. *Nat Rev Neurosci* 8: 623–635, 2007.

**Long MA, Fee MS.** Using temperature to analyse temporal dynamics in the songbird motor pathway. *Nature* 456: 189–194, 2008.

**Mavoori J, Jackson A, Diorio C, Fetz E.** An autonomous implantable computer for neural recording and stimulation in unrestrained primates. *J Neurosci Methods* 148: 71–77, 2005.

**McDermott H.** An advanced multiple channel cochlear implant. *IEEE Trans Biomed Eng* 36: 789–797, 1989.

**Moritz CT, Perlmutter SI, Fetz EE.** Direct control of paralysed muscles by cortical neurons. *Nature* 456: 639–642, 2008.

**Nottebohm F, Stokes TM, Leonard CM.** Central control of song in the canary, *Serinus canarius*. *J Comp Neurol* 165: 457–486, 1976.

**Peng C-W, Chen J-JJ, Lin C-CK, Poon PW-F, Liang C-K, Lin K-P.** High frequency block of selected axons using an implantable microstimulator. *J Neurosci Methods* 134: 81–90, 2004.

**Salzman CD, Britten KH, Newsome WT.** Cortical microstimulation influences perceptual judgements of motion direction. *Nature* 346: 174–177, 1990.

**Sarpeshkar R, Wattanapanich W, Arfin SK, Rapoport BI, Mandal S, Baker MW, Fee MS, Musallam S, Andersen RA.** Low-power circuits for brain-machine interfaces. *IEEE Trans Biomed Circuits Syst* 2: 173–183, 2008.

**Sit J-J, Sarpeshkar R.** A low-power blocking-capacitor-free charge-balanced electrode-stimulator chip with less than 6 nA DC error for 1-mA full-scale stimulation. *IEEE Trans Biomed Circuits Syst* 1: 172–183, 2007.

**Sossinka R, Böhner J.** Song types in the zebra finch (*Poephila guttata castanotis*). *Z Tierpsychol* 53: 123–132, 1980.

**Swadlow HA.** Neocortical efferent neurons with very slowly conducting axons: strategies for reliable antidromic identification. *J Neurosci Methods* 79: 131–141, 1998.

**Talwar SK, Xu S, Hawley ES, Weiss SA, Moxon KA, Chapin JK.** Rat navigation guided by remote control. *Nature* 417: 37–38, 2002.

**Tarsy D, Vitek JL, Starr PA, Okun MS.** *Deep Brain Stimulation in Neurological and Psychiatric Disorders*. Clifton, NJ: Humana Press, 2008.

**Theogarajan LS.** A low-power fully implantable 15-channel retinal stimulator chip. *IEEE J Solid-State Circuits* 43: 2322–2337, 2008.

**Tsividis Y.** *Operation and Modeling of the MOS Transistor* (2nd ed.). New York: Oxford Univ. Press, 1999.

**Vu ET, Mazurek ME, Kuo YC.** Identification of a forebrain motor programming network for the learned song of zebra finches. *J Neurosci* 14: 6924–6934, 1994.

**Wang CZ, Herbst JA, Keller GB, Hahnloser RH.** Rapid interhemispheric switching during vocal production in a songbird. *PLoS Biol* 6: e250, 2008.

**Wattanapanich W, Fee M, Sarpeshkar R.** An energy-efficient micropower neural recording amplifier. *IEEE Trans Biomed Circuits Syst* 1: 136–147, 2007.